Observation of Reversible Pore Change in Mesoporous Tin Phosphate Anode Material during Li Alloying/Dealloying

Hansu Kim,[a] Gyeong-Su Park,[b] Eunjin Kim,[c] Jinyoung Kim,[c] Seok-Gwang Doo,[a] and Jaephil Cho[c,*,z]

[a]Materials Laboratory and [b]Analytical Engineering Center, Samsung Advanced Institute of Technology, Giheung, Korea
[c]Department of Applied Chemistry, Kumoh National Institute of Technology, Gumi, Korea

We observed the pore expansion and contraction of mesoporous tin phosphate during Li alloying/dealloying using small-angle X-ray scattering and transmission electron microscopy. As-prepared mesoporous tin phosphate showed pore and porewall sizes of 3 and 2 nm, respectively. During lithium alloying (discharging), pore size was slightly contracted, but porewall size was slightly expanded within the range of 1 nm. However, during lithium dealloying (charging), pore and porewall sizes recovered to their original sizes before cycling. The charged sample had a nanoscale pore (~3 nm) array with a more or less uniformly sized open-porewall structure of amorphous lithium phosphates with metallic α-Sn face-centered-cubic nanocrystals ~2 nm in diameter.
© 2006 The Electrochemical Society. [DOI: 10.1149/1.2212061] All rights reserved.

Metal phosphates have been heavily studied in the area of $AlPO_4$ for catalytic applications, but little progress has been made with other types of phosphates.[1-4] Recently, surfactant-mediated SnO_2 and tin phosphates have been reported as having possible application in Li rechargeable batteries.[5-7] Mesoporous and crystalline composites consisting of tin phosphates with a Brunauer–Emmett–Teller (BET) surface area of 76 m^2/g exhibited initial charge capacity of ~600 mAh/g with an irreversible capacity ratio of 25%.[5] Further, these materials showed <10% capacity fading after 30 cycles compared to other lithium reactive metal oxides that underwent severe capacity losses. It has been proposed that the excellent capacity retention was possibly due to reversible pore changes during the Li reaction. Kim et al. have reported that tin phosphate was first decomposed to an active $Li_{4.4}Sn$ alloy and an inactive amorphous lithium phosphate phase.[5] A similar mechanism was also proposed by Courtney and Dahn[8,9] and Xiao et al.[10] Despite these studies, no direct evidence for pore and porewall changes or the formation of tin particles in the porewall framework during Li alloying/dealloying has been discovered.

Here, we report a systematic observation of pore structure changes in mesoporous tin phosphate during Li alloying/dealloying.

Experimental

Mesoporous tin phosphate was prepared by mixing 9.0 g SnF_2 and 12 g H_3PO_4 followed by dissolution in distilled-deionized water (DDW). Twelve grams of sodium dodecyl sulfate (SDS) was dissolved in 40 mL of DDW, and this solution was added to a solution of SnF_2 and H_3PO_4. The mixture was stirred at 40°C for 1 h and then maintained in an autoclave at 90°C for 5 days. After cooling to room temperature, the precipitate was recovered by filtration, washed with distilled water and ethanol, and vacuum-dried at 100°C for 10 h. The powders were annealed at 500°C for 5 h, yielding a mesoporous tin phosphate phase. The procedure for assembling a coin-type half-cell with Li as the anode is described in detail elsewhere.[11,12] Generally, the area of the electrode was 2 cm^2 and contained 20 mg tin phosphate powder and 2 mg polyvinylidene fluoride. A mixture of ethylene carbonate/diethylene carbonate (EC/DEC) and 1 M $LiPF_6$ salts was used as the electrolyte. After assembling the cells, they were discharged and charged to 0 and 1.5 V, respectively. The electrodes were detached from the cells, rinsed several times with a dimethyl carbonate (DMC) solution, and then the binder was removed in an N-methyl-2-pyrrolidone (NMP) solution. The solution was filtered and the sample was washed with acetone several times for microstructural analysis. The small-angle X-ray scattering (SAXS) patterns were obtained using a Rigaku instrument. The nitrogen adsorption isotherm was measured at 77 K on a Micromeritics ASAP 2010 gas sorption system.

Results and Discussion

Figure 1a shows the SAXS patterns of the as-prepared mesoporous tin phosphate after annealing at 500°C for 5 h. The intense peak of the as-synthesized mesoporous tin phosphate corresponds to the d-spacing of 5.0 ± 0.2 nm (from $2d \sin \theta = \lambda$). Similar single-peak diffraction patterns with small d-spacing were previously observed in SnO_2 and tin phosphates.[7,12,13] An as-prepared sample shows a relatively sharp peak, indicating a high degree of pore ordering. However, SAXS patterns of the samples discharged and charged to 0 and 1.5 V, respectively, show somewhat broader peaks, indicating a disordered pore structure. Even in mesoporous materials with very low degrees of pore ordering, SAXS showed these peaks.[4,7,14] The broad high-angle X-ray diffraction (XRD) pattern (Fig. 1 inset, curve d) indicates that the tin phosphate consists of either amorphous or possibly nanocrystalline mesoporous walls. Curves b and c in Fig. 1 exhibit the SAXS patterns of the mesoporous tin phosphate after discharging and charging to 0 and 1.5 V,
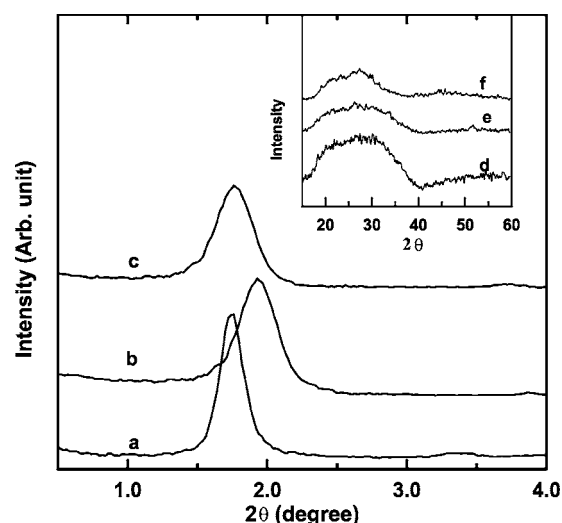

Figure 1. SAXS diffraction patterns of (a) as-prepared, (b) discharged, and (c) charged tin phosphates to 0 and 1.5 V, respectively. Insets of (d), (e) and (f) are wide-angle XRD patterns of (a), (b), and (c), respectively.

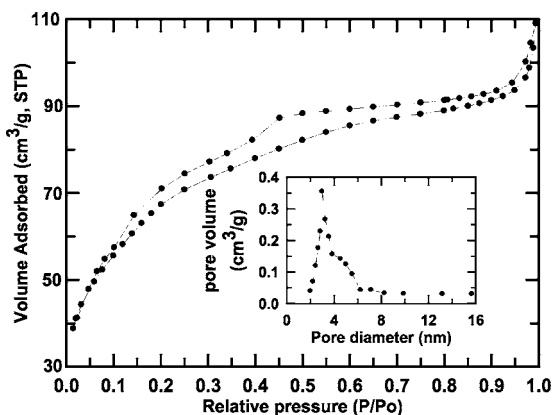* Electrochemical Society Active Member.
z E-mail: jpcho@kumoh.ac.kr

Figure 2. Nitrogen adsorption–desorption isotherms and pore-size distribution (inset) for as-prepared tin phosphate.

Figure 3. (a) Potential profiles of mesoporous tin phosphates in a coin-type half-cell as a function of cycle number between 0 and 1.5 V at a rate of 200 mA/g. (b) Differential plot of (a).

respectively. The discharged sample showed that the peak had shifted to a higher 2θ angle, indicating that the mesoperiodicity of the annealed mesoporous tin phosphate contracted, corresponding to a *d*-spacing of 4.5 ± 0.2 nm. After charging to 1.5 V, the mesopore array material expanded, showing a *d*-spacing value of 5.0 ± 0.3 nm, which is quite similar to that of the as-prepared sample. However, the *d*-spacing trend of the discharged and charged samples is opposite that of the mesoporous/crystalline composite consisting of tin phosphate reported by Kim et al.[5] This finding may be associated with the different nature of the porewall frame structure, and further investigation into the origin of this difference using transmission electron spectroscopy is in progress.

Figure 2 exhibits N_2 adsorption and desorption isotherms of the as-prepared sample. Barrett–Joyner–Halenda (BJH) analysis[15] (inset) confirmed well-ordered mesoporous tin phosphate with a pore size of 3 nm. Its BET specific surface area was 200 m²/g, which is a quite reasonable value compared with other mesoporous oxides such as TiO_2, SnO_2, tin phosphate, and iron phosphates with BET surface areas of ~150–200 m²/g.[13,16,17]

Figure 3 shows cycling performances between 1.5 and 0 V of the mesoporous tin phosphate in a coin-type half-cell at a rate of 200 mA/g. The first charge capacity was 610 mAh/g, with a large irreversible capacity of 662 mAh/g, and capacity retention after 40 cycles was 93% of the first charge capacity. This capacity retention is far superior to that of previously reported anode materials, such as amorphous or crystalline-tin-containing oxides.[18-20] Differential capacity plots (Fig. 3b) of the coin-type half-cell containing mesoporous tin phosphate were constructed from the corresponding cycling curves in Fig. 3b. The sharp peak at 1.2 V during the first discharge is related to the reduction of the tin phosphate to tin and lithium phosphate phases. The peaks at around 0.2 and 0.5 V are lithium insertion/extraction reactions associated with lithium-tin alloy phases of different compositions. As the differential capacity plots are sensitive detectors of change in the voltage profiles from cycle to cycle, the constancy of the plots is indicative of the good reversibility of the electrode material in repetitive charge and discharge operations. However, maintaining broad peaks out to 40 cycles indicates that tin nanoparticles are confined in the porewall frameworks without growing into large clusters. This observation contrasts with that of tin and tin oxide composite glasses reported by Courtney and Dahn.[18] Their $dq/d(mdV)$ was smooth for the first six cycles but turned into strong sharp peaks after 15 cycles, indicating the formation of large tin clusters.

In order to obtain more information on the pore size distribution and BET surface area of the discharged and charged samples, N_2 adsorption and desorption isotherm tests were carried out. Figure 4a and b shows the N_2 adsorption and desorption isotherms of the discharged and charged tin phosphate, respectively, that are charac-
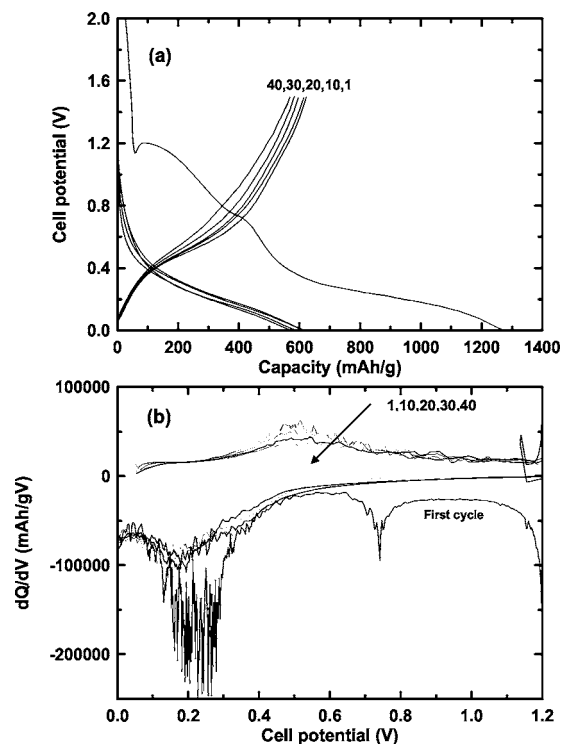
teristic of framework-confined mesopores. BJH analysis of the discharged and charged samples indicates pore sizes of 2 and 3 nm, respectively (Fig. 4a and b insets). BET specific surface area of the discharged and charged samples was 198 and 205 m²/g, respectively. During lithium alloying (discharging), pore size was slightly contracted by 0.5 nm, while it expanded slightly within the range of 1 nm. Hence, we believe that BET surface area did not change significantly. Porewall size can be directly estimated from the difference between *d*-spacing and pore size values. Therefore, porewall size of the discharged and charged samples can be deduced to be 2.5 and 2 nm, respectively. The results showed that the initial pore size of 3 nm was slightly contracted to 2.5 nm, but the pore wall size of 2 nm was slightly expanded to 2 nm after discharging. Hence, the volume change is negligible compared with that of SnO_2 or Sn particles which show 300% volume increase, resulting in particle aggregation and pulverization. The broadened SAXS peak of the charged sample shows partial destruction of the mesopore ordering despite the maintenance and stability of the mesopore structure during the discharge–charge cycle.

The broad peak near ~25° in curves e and f (discharged and charged tin phosphate, respectively) in Fig. 1 is believed to stem from the amorphous lithium phosphates matrix. The formation of the amorphous lithium phosphates phase during lithium alloying/dealloying was reported by Xiao et al.[10] In addition, it has been reported that the $Li_{4.4}Sn$ and Sn phases at 0 and 1.5 V, respectively, showed major peaks between 20 and 32° in the XRD patterns.[9,21] However, our XRD patterns did not show any peaks, indicating that the $Li_{4.4}Sn$ and Sn phases did not grow into enough larger clusters to be detectable by XRD.

The major challenge in obtaining mesoporous oxides is to preserve the mesoporous structure while the surfactant is being removed during annealing. In order to avoid severe coarsening or collapsing of the mesostructure, it is necessary to form a rigid, three-dimensional, inorganic framework based on Sn-O-P bonding before removing the surfactant. In our material, it is believed that the
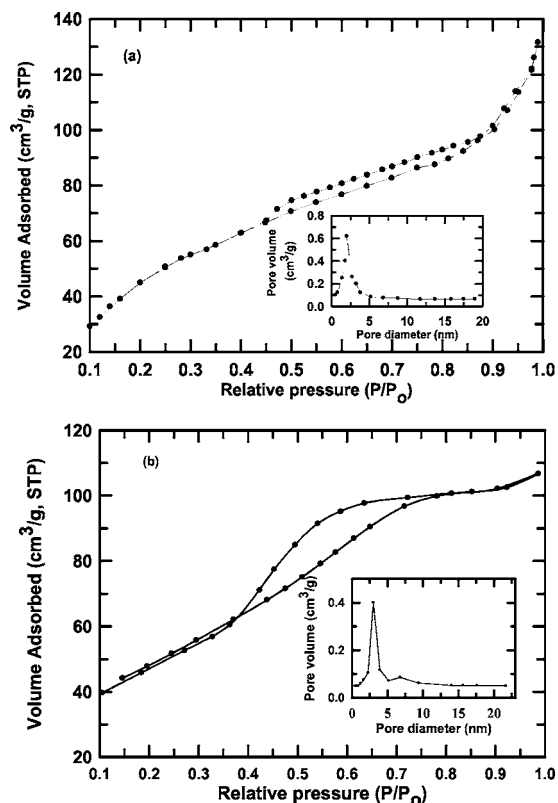
Figure 4. Nitrogen adsorption–desorption isotherms and pore-size distribution (inset) for (a) discharged and (b) charged tin phosphate to 0 and 1.5 V, respectively. The sample was outgassed overnight at 150°C prior to analysis.

Figure 5. (a) Electron probe image of the nanocrystals in the charged tin phosphate sample as indicated by the arrows. (b) NED pattern from the nanocrystalline area containing amorphous lithium phosphate. (c) Radial intensity profile of the NED pattern (Fig. 5b) obtained from the area of the nanocrystals.

Sn-O-P bonds are formed during the aging process through water condensation. Once a condensed, 3D mesoporous network is formed, its essential mesoporous features are likely to be preserved after removing the surfactant at 500°C.

In order to confirm the formation of Sn nanoparticles in the charged sample to 1.5 V, coherent nanoarea electron diffraction (NED) techniques were applied.[22] The high angular resolution and the small probe size of the NED allowed us to directly determine the structure of very small nanoparticles. Figure 5a shows the electron probe image of the nanocrystals in the charged tin phosphate as indicated by the arrows. The electron probe was measured to be 50 nm in diameter, which was sufficient to obtain a high intensity of NED patterns from the area of nanocrystals. Figure 5b shows two additional bright diffraction rings (marked 1 and 2 in the right figure of Fig. 5b) from small nanoparticles. Radial intensity distribution analysis of the NED pattern was performed to measure the atomic distance of rings 1 and 2. Figure 5c shows the radial intensity profile of the NED pattern obtained from the area of nanocrystals. The reciprocal distances of peaks 1 and 2 measured from the profile were 2.67 nm^{-1} (3.75 Å) and 5.13 nm^{-1} (1.95 Å), which corresponded to the (111) and (311) reflections of α-Sn (face-centered-cubic), respectively. The Sn nanocrystals are electrochemically formed from the amorphous lithium phosphate framework during Li dealloying, and the porewall structure is effectively conserved without collapsing during the discharge/charge cycle.

Conclusion

We observed reversible changes in the pore and porewall of tin phosphate during lithium alloying/dealloying, within a range of <1 nm. Even after charging to 1.5 V, mesopore order was well preserved, and ~2 nm sized tin particles were grown in the porewall framework.
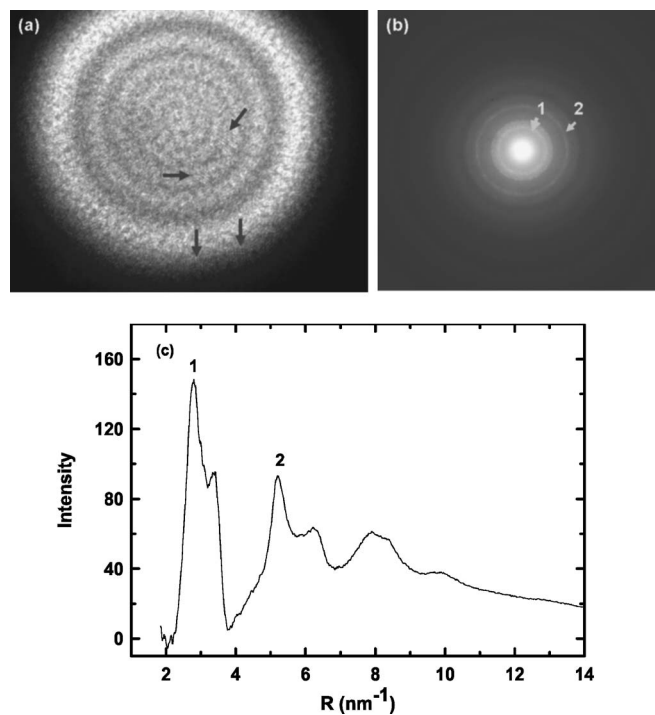
References

1. J. El Haskouri, R. S. Cabrera, M. Bertran-Polter, D. Beltranpoter, M. D. Marcos, and P. Amoros, *Chem. Mater.*, **11**, 1446 (1999).
2. C. Serre, C. Magnier, M. Hervieu, F. Taulelle, and G. Ferey, *Chem. Mater.*, **14**, 180 (2002).
3. C. Serre, A. Auroux, A. Gervasini, M. Hervieu, and G. Ferey, *Angew. Chem., Int. Ed. Engl.*, **35**, 541 (1996); *Angew. Chem., Int. Ed.*, **41**, 1594 (2004).
4. J. Y. Ying, C. P. Mehnert, and M. S. Wong, *Angew. Chem., Int. Ed.*, **38**, 56 (1999).
5. E. Kim, D. Son, T.-G. Kim, J. Cho, B. Park, K. S. Ryu, and S. H. Chang, *Angew. Chem., Int. Ed.*, **43**, 5987 (2004).
6. E. Kim, M. G. Kim, and J. Cho, *Electrochem. Solid-State Lett.*, **8**, A452 (2005).
7. F. Chen and M. Liu, *Chem. Commun. (Cambridge)*, **1999**, 1829.
8. I. A. Courtney and J. R. Dahn, *J. Electrochem. Soc.*, **144**, 2943 (1997).
9. I. A. Courtney and J. R. Dahn, *J. Electrochem. Soc.*, **144**, 2045 (1997).
10. Y. W. Xiao, J. Y. Lee, A. S. Yu, and Z. L. Liu, *J. Electrochem. Soc.*, **146**, 3623 (1999).
11. J. Cho, Y. J. Kim, T.-J. Kim, and B. Park, *Angew. Chem., Int. Ed.*, **40**, 3367 (2001).
12. J. Cho, Y.-W. Kim, B. Kim, J.-G. Lee, and B. Park, *Angew. Chem., Int. Ed.*, **42**, 1618 (2003).
13. N. K. Mal, S. Ichikawa, and M. Fujiwara, *Chem. Commun. (Cambridge)*, **2002**, 112.
14. S. Cabrera, J. E. Haskouri, J. Alamo, A. Beltran, D. Beltran, S. Mendioroz, M. D. Marcos, and P. Amoros, *Adv. Mater. (Weinheim, Ger.)*, **1**, 379 (1999).
15. P. A. Webb and C. Orr, *Analytical Methods in Fine Particle Technology*, Micromeritics Instruments Corp., Norcross, GA (1997).
16. X. Guo, W. Ding, X. Wang, and Q. Yan, *Chem. Commun. (Cambridge)*, **2001**, 709.
17. P. Yang, D. Zhao, D. I. Margolese, B. F. Chmelka, and G. D. Stucky, *Nature*

   (London), **396**, 152 (1998).
18. I. A. Courtney, W. R. Mckinnon, and J. R. Dahn, *J. Electrochem. Soc.*, **146**, 59 (1999).
19. K. Wan, S. F. Y. Li, Z. Gau, and K. S. Siow, *J. Power Sources*, **75**, 9 (1998).

20. M. Behm and J. T. S. Irvine, *Electrochim. Acta*, **47**, 1727 (2002).
21. C. Kim, M. Noh, M. Choi, J. Cho, and B. Park, *Chem. Mater.*, **17**, 3297 (2005).
22. J. M. Zuo, M. Gao, J. Tao, B. Q. Li, R. Twesten, and I. Petrov, *Microsc. Res. Tech.*, **64**, 347 (2004).